Risk-based Fatigue Design Considering Inspections and Maintenance

Jorge Mendoza[1], Elizabeth Bismut[2], Daniel Straub[3], and Jochen Köhler[4]

[1]PhD student, Department of Structural Engineering, Norwegian University of Science and Technology, 7491 Trondheim, Norway. Email: jorge.m.espinosa@ntnu.no

[2]PhD student, Engineering Risk Analysis Group, Technische Universität München, 80290 München, Germany. Email: elizabeth.bismut@tum.de

[3]Professor W2, Engineering Risk Analysis Group, Technische Universität München, 80290 München, Germany. Email: straub@tum.de

[4]Professor, Department of Structural Engineering, Norwegian University of Science and Technology, 7491 Trondheim, Norway. Email: jochen.kohler@ntnu.no

ABSTRACT

The different phases of a structure's life-cycle are managed by different teams with little interaction. Correspondingly, the optimization of the individual phases is isolated and does not necessarily result in optimal life-cycle decisions. This motivates the treatment of structural optimization from a broader life-cycle perspective. A framework to enhance the design of structural systems by considering the operation and maintenance phase in the decision process is proposed in this article. The framework focuses on fatigue prone details, but it can be extended to consider other deterioration mechanisms. A hierarchical influence diagram is proposed as an efficient way to represent the probabilistic decision problem while considering system effects, such as the correlation of the deterioration among hot-spots. A simple example is presented to illustrate the implementation of the framework. Challenges and potential applications are discussed.

INTRODUCTION

A significant share of the available societal resources is spent annually to develop new public infrastructure and to manage the existing one. For instance, European countries employed on average 3.3%-4.2% of their GDP in gross fixed capital formation (GFCF) during 2009-2015 (Athenosy et al. 2017), the USA spent 2.4% of GDP in 2014 (Shirley, Chad 2017), and Canada spent 7.4% of GDP during 1956-1993 (Kalaitzidakisa and Kalyvitisb 2005). The investment in operation and maintenance (O&M) constitutes a large part of this expenditure. By way of example, Canada employed on average 21% of the GFCF in O&M during 1956-1993 (Kalaitzidakisa and Kalyvitisb 2005), while the USA spent on average 49% during 1956-2004 (Rioja 2013). The built environment is reaching a state of maturity in developed countries and the cost associated with the integrity management of existing infrastructure is increasing its share of the total expenditure in public infrastructure. As a reference, it is estimated by using the database from the US Department of Transportation (FHWA 2020) that the ratio between the number of highway bridges subject to major repair or reconstruction to newly constructed ones increased from 7% during the 1950s, to 13% during the 1970s and to 24% during the 2000s.

For a particular structure, the main phases of its life-cycle are (see Figure 1) (i) planning and design, (ii) construction/installation, (iii) commissioning, (iv) O&M, and (v) decommissioning. Integrity management, including the planning of inspections and maintenance (I&M), is a crucial part of the life-cycle optimization of structures. Optimal I&M planning for a structural system depends on many aspects specified during the design phase: number and configuration of structural components, accessibility of hot-spots, correlation of the material resistance among components, importance of components relative to system reliability, redundancy and robustness. Correspondingly, the consideration of possible integrity management measures in structural design decisions likely results in a more optimal use of resources (ISO 2015; McAuliffe et al. 2017).

Life-cycle risk management for fatigue deteriorating structures

Decisions made for the integrity management of structures depend on the estimation of their structural reliability. The reliability of a structural system changes with time. Deterioration processes, such as corrosion or fatigue, may reduce the structural resistance during the operational life of the structure. Moreover, the stochastic environmental loading may not be a stationary process. The estimation of structural reliability is conditional on the available knowledge. Consequently, information acquisition techniques that reduce uncertainty, such as inspections and structural health monitoring, have a strong influence on the estimation of structural reliability and correspondingly on integrity management decisions.

This study focuses on fatigue deterioration. The current practice for fatigue assessment is established in several standards and recommended design guidelines, e.g. NORSOK 2004; HSE 1995; CEN 2005; ISO 2007; API 2002; Hobbacher 2016; DNV-GL 2016; BSI 2015. An overview of the fatigue assessment approaches and safety factors employed in some of these standards can be found in HSE (2001). In general, these codes provide prescriptive rules for fatigue design based on a semi-probabilistic safety format. Often, different safety factors are given depending on the consequences of failure. For instance, three different consequence classes are distinguished by the International Institute of Welding (Hobbacher 2016): (1) loss of secondary structural parts, (2) loss of entire structure and (3) loss of human life.

Risk of failure can be managed throughout the different phases of a structure's life-cycle. The definition of risk and the information that is required for its computation may differ depending on the type of decision that is assessed. For instance, the assessment of the risk of fatigue failure at the design phase is in general assessed using semi-empirical SN-curves (DNV-GL 2016), whereas the fracture mechanics approach is preferred during O&M (Almar-Næss 1985; DNV-GL 2015). The latter is due to the need of relating fatigue deterioration to physical parameters, such as crack depth, that are directly observable and can consequently be updated based upon structural health information. To represent the sequential decision problem that includes design as well as I&M decisions, coherent probabilistic models of the relevant phenomena should be chosen.

Fatigue design of steel structures is addressed in part 1-9 of the Eurocode 3 (CEN 2005). The code accepts two different design approaches: (1) safe-life and (2) damage tolerant. Partial safety factors are provided for two levels of inspectability or accessibility to the structural detail:

accessible joint detail and poor accessibility.

(1) The safe-life method dispenses with regular inspections by requiring a sufficiently large reliability level. This is achieved by reducing the probability of a crack growing to a critical crack dimension below a codified threshold during the service life of the structure (Gurney 1979).

(2) For the damage tolerant method, also called the fail-safe approach, structures are designed such that cracks are expected to develop at certain hot-spots. It was developed by the aircraft industry for the purpose of reducing the amount of employed structural material and therefore, reducing the weight of the aircrafts (Lincoln 1985). Consequently, regular inspections are required in order to maintain the structure within a reasonable safety-level during its service life.

The damage tolerant approach opens the possibility of finding a cost-optimum balance between the investments in maintenance and design. Nevertheless, the required level of safety at design in Eurocode 3 is prescribed independently from an inspection and maintenance program.

Integrated structural design and life-cycle integrity management

Extensive literature exists on the development and application of risk-based methodologies for the different phases of a structure's life-cycle. A comprehensive overview is presented in Moan (2018) for offshore structures. However, there are not many studies conducted on quantitative design methodologies that address the combined impact and efficiency of mitigation measures performed at different points in time of the life-cycle of a structure. These methods are referred to as integrated structural design methods in this paper. A review of literature in this field is presented in the following.

The usefulness of integrating I&M information at the design phase is emphasized in the literature (Straub et al. 2006; Moan 2018). A model to quantify the effect of fatigue design on inspection planning at the component level is proposed in Madsen and Sorensen (1990). The framework is applied to the optimization of the thickness, inspection times and inspection quality of a jacket joint. Cramer and Friis-Hansen (1994) use this model to address optimal design, fabrication and inspection length for welded components with several hot-spots. Moan et al. (1993) proposes a relaxation of the design Palmgren-Miner's sum as a function of the inspection program. Generic reliability- and risk-based inspection planning methods have been developed in terms of commonly used deterministic design parameters, such as the fatigue design factor *FDF* defined in this paper in Eq. (7) (Faber et al. 2000; Straub 2004; Faber et al. 2005). Some system effects were neglected in these studies, such as the updating of a component due to the inspection outcome of nearby components; although other system considerations were included, such as the importance of a component with regard to the integrity of the system. Straub et al. (2006) shows the benefits of risk-based inspection (RBI) planning for offshore structures and discusses the possibility of optimising inspection planning and the *FDF* by including the associated construction costs. In Sørensen (2011) and Márquez-Domínguez and Sørensen (2012), a framework for reliability-based *FDF* calibration for offshore wind turbines is developed. Another application of this framework exists for RBI planning of a 20 MW offshore wind turbine jacket (Gintautas et al. 2018). A component based optimization of the *FDF* and maintenance strategy is proposed in Zou et al. (2018). A risk-based framework for conceptual design of ships is developed in Garbatov et al. (2018), where an ultimate limit state is considered in combination with deterioration due to corrosion.

In summary, models to quantify the effect of design on life-cycle risk and on optimal I&M planning exist in the literature. Furthermore, reliability requirements for I&M given design specifications are provided in studies and design standards. Models to simultaneously assess optimal integrated design and I&M strategies began to be developed in the 90s for the component level. Little follow-up of these studies is documented in the literature afterwards, although new studies from the offshore wind sector have been published in recent years. The authors are not aware of studies on optimal integrated fatigue design and I&M planning methods at the system level.

Aim of the paper

The objective of this paper is to present a risk-based integrated structural design framework in which I&M planning of deteriorating details is explicitly considered. The framework considers system effects such as the effect of correlation among hot-spot deterioration, the level of redundancy and the impact of information gathered at the component level on system reliability. The proposed framework is elaborated in the following section. Afterwards, the methodology is implemented to study the optimal life-cycle fatigue design of the joints of a lattice structure. Advantages and limitations of the proposed methodology are explored, together with some potential applications of the framework and further research. The paper concludes with a summary of the main findings.

INTEGRATED STRUCTURAL DESIGN FRAMEWORK

The proposed framework aims to optimise the allocation of mitigation measures during the life-cycle of deteriorating structural systems prior to their construction. Two mitigation measures are considered. Namely, to increase the safety level at the design phase and to conduct I&M actions. The framework explicitly addresses system effects. This is computationally demanding (Luque and Straub 2016). Consequently, an efficient system representation needs to be used. The proposed framework is kept general in this section, but a hierarchical influence diagram (ID) based on Luque and Straub (2019) and Bismut and Straub (2018) is employed for the numerical example in the following section. The computational demand of the numerical example is reported in the discussion section.

Generic representation

The proposed framework is illustrated in Figure 2. An integrated design is here defined as the combination of a design specification $\mathcal{D}_j \in \boldsymbol{\mathcal{D}}$ together with an I&M strategy $\mathcal{S}_i \in \boldsymbol{\mathcal{S}}$. A design consists of a set of specifications that are sufficient to assess the safety level of the structural system for given failure mechanisms. An I&M strategy specifies when and where to inspect as well as the repair and maintenance criteria. The optimal integrated design $\{\mathcal{D}_{opt}, \mathcal{S}_{opt}\}$ is defined as the one that minimizes the expected total life-cycle cost.

In their most complete definition, $\boldsymbol{\mathcal{D}}$ and $\boldsymbol{\mathcal{S}}$ would contain all possible design descriptions and I&M strategies. Nevertheless, this is unpractical and therefore, smart choices should be made upfront to explore a reduced, yet still representative, space of alternatives. For instance, $\boldsymbol{\mathcal{D}}$ could contain a discrete set of fatigue safety factor values. $\boldsymbol{\mathcal{S}}$ could contain decision rules, such as repair any detected damage, and a reduced set of alternatives, such as a set of time intervals between preventive inspections (Bismut and Straub 2020). Optimal I&M planning given a design specification depends on available information and therefore, it can and should be reassessed for the as-built structure and every time new information becomes available (Madsen and Sorensen 1990; Moan 2018). This is to be considered in the selection of the appropriate level of detail used to represent potential I&M strategies.

The system representation includes:

- A deterioration model that allows for the representation of the influence on the deterioration process of design decisions and maintenance actions.
- A model for the statistical dependence of the deterioration among components, since this affects the estimation of the reliability of the system and the efficiency of the inspection campaigns.
- A likelihood model connecting the observations from the inspection techniques with the state of deterioration.
- A model that relates component condition to system reliability.
- A model for the costs of the different decision alternatives and consequences of the considered outcomes.

Objective function

A set of N_d designs $\boldsymbol{\mathcal{D}} = \{\mathcal{D}_1, \mathcal{D}_2, ..., \mathcal{D}_{N_d}\}$ and a set of N_s I&M strategies $\boldsymbol{\mathcal{S}} = \{\mathcal{S}_1, \mathcal{S}_2, ..., \mathcal{S}_{N_s}\}$ are considered. The optimal integrated design $\{\mathcal{D}_{opt}, \mathcal{S}_{opt}\}$ is found by minimizing the expected life-cycle cost $\mathrm{E}[C_T(\mathcal{D}_j, \mathcal{S}_i)]$:

$$\{\mathcal{D}_{opt}, \mathcal{S}_{opt}\} = \underset{\substack{i=1,...,N_s;\\ j=1,...,N_d}}{\arg\min}\{\mathrm{E}[C_T(\mathcal{D}_j, \mathcal{S}_i)]\} \tag{1}$$

where $\mathrm{E}[\cdot]$ is the expectation operator.

The expected life-cycle cost $\mathrm{E}[C_T(\mathcal{D}_j, \mathcal{S}_i)]$ is defined as the sum of the design cost $C_D(\mathcal{D}_j)$, which includes costs associated with the design and construction of the structural components, and the expected inspection, maintenance and failure (IMF) cost $\mathrm{E}[C_{IMF}(\mathcal{D}_j, \mathcal{S}_i)]$:

$$\mathrm{E}[C_T(\mathcal{D}_j, \mathcal{S}_i)] = C_D(\mathcal{D}_j) + \mathrm{E}[C_{IMF}(\mathcal{D}_j, \mathcal{S}_i)] \tag{2}$$

The expected IMF cost $\mathrm{E}[C_{IMF}(\mathcal{D}_j, \mathcal{S}_i)]$ is computed as the sum of the expected costs associated with starting an inspection campaign C_C, conducting inspections C_I, repairs C_R and failure C_F:

$$\mathrm{E}[C_{IMF}(\mathcal{D}_j, \mathcal{S}_i)] = \mathrm{E}[C_C(\mathcal{D}_j, \mathcal{S}_i)] + \mathrm{E}[C_I(\mathcal{D}_j, \mathcal{S}_i)] + \mathrm{E}[C_R(\mathcal{D}_j, \mathcal{S}_i)] + \mathrm{E}[C_F(\mathcal{D}_j, \mathcal{S}_i)] \tag{3}$$

These costs are discounted to their present value by a function $\gamma(t)$ as described in (Bismut and Straub 2020). In particular, the expected failure cost, also called risk of failure R_F, is given by:

$$R_F(\mathcal{D}_j, \mathcal{S}_i) = \mathrm{E}_Z\left[\mathrm{E}_\Theta[C_F(\mathcal{D}_j, \mathcal{S}_i|\mathbf{Z})]\right] = \mathrm{E}_Z\left[\sum_{t=1}^{T_{SL}} C_F \cdot \gamma(t) \cdot \Pr(F_{sys,yr,t}|\mathbf{Z}_{0:t-1})\right] \tag{4}$$

where C_F is the cost of failure and $\Pr(F_{sys,yr,t}|\mathbf{Z}_{0:t-1})$ is the annual probability of failure during year $t-1$ to t, conditional on available information up to time $t-1$, denoted $\mathbf{Z}_{0:t-1}$. The expectation over the cost of failure is computed over possible states of the system $\boldsymbol{\Theta} \in \Omega_\Theta$ and inspection outcomes $\mathbf{Z} \in \Omega_Z$. This double expectation is computationally expensive. Luque and Straub (2019) propose to first compute the expected cost of failure conditional on the inspection outcomes and afterwards integrate over the sampled observation histories by crude Monte Carlo simulations (MCS). A relatively low number of samples is needed since the conditional probability of failure is computed for each sampled observation history. They estimate that around $n_{sim} = 200$ simulations suffice for most practical applications, although this depends on the variance of the expected cost of failure conditional on the observation histories, i.e. $\mathrm{Var}_Z[\mathrm{E}_\Theta[C_F(\mathcal{D}_j, \mathcal{S}_i|\mathbf{Z})]]$. The accuracy of the estimation is explored below for the numerical application.

The minimisation of the expected life-cycle cost in Eq. (1) can be divided into two steps, as illustrated in Figure 2. First, an optimal strategy $\mathcal{S}_{opt,j}$ can be found given a certain design specification $\mathcal{D}_j$ through the minimization of the expected IMF cost:

$$\mathcal{S}_{opt,j} = \mathcal{S}_{opt}|\mathcal{D}_j = \underset{i=1,...,N_s}{\arg\min}\{\mathrm{E}[C_{IMF}(\mathcal{S}_i, \mathcal{D}_j)]\} \tag{5}$$

For N_d considered designs, the set of optimal strategies is collected into the vector $\hat{\boldsymbol{\mathcal{S}}}_{opt} = \{\hat{\mathcal{S}}_{opt,1}, \hat{\mathcal{S}}_{opt,2}, ..., \hat{\mathcal{S}}_{opt,N_d}\}$. The optimal integrated design $\mathcal{D}_{opt} \in \boldsymbol{\mathcal{D}}$ and $\mathcal{S}_{opt} \in \hat{\boldsymbol{\mathcal{S}}}_{opt}$ is then computed as:

$$\{\mathcal{D}_{opt}, \mathcal{S}_{opt}\} = \underset{j=1,...,N_d}{\arg\min}\{\mathrm{E}[C_T(\mathcal{D}_j, \hat{\mathcal{S}}_{opt,j})]\} \tag{6}$$

DESCRIPTION OF THE CASE STUDY

The application of the proposed framework is illustrated with a case study. The fatigue design of the joints of the offshore lattice structure in Figure 3 is considered. The structure is a redundant frame constituted of six tubular members (B1-B6) and a semi-rigid top horizontal I-beam. All joints among members are welded. The frame structure has ten locations or hot-spots (HS1-HS10) where fatigue cracks may occur under cyclic loading. Hot-spots above the highest astronomical tide (HAT), i.e. HS1-HS4, are denoted dry hot-spots and can be inspected. Hot-spots HS5-HS10 are denoted submerged hot-spots and are assumed to be non-accessible, i.e. they cannot be inspected. The frame is subject to an extreme environmental load with annual maximum Q and cyclic wave loading $L(t)$. The system is a simple structure that allows investigating the effect of:

(1) the correlation among component deterioration;
(2) the structural importance of the components;
(3) the inspectability of structural details.

The objective of the decision problem is to compute the optimal integrated fatigue design of the structure $\{\mathcal{D}_{opt}, \mathcal{S}_{opt}\}$. An inspection strategy $\mathcal{S}_j$ is characterized by the time between inspection campaigns Δt_I. A fatigue design $\mathcal{D}_j$ is characterised by the specification of the fatigue design factor *FDF* of the hot-spots. The *FDF* of a hot-spot i is defined as the ratio between its deterministic fatigue life $T_{FL,i}$ and the design service life of the structure $T_{SL} = 20$ years:

$$FDF_i = \frac{T_{FL,i}}{T_{SL}} \tag{7}$$

Hierarchical influence diagram

A hierarchical ID is used to assess the influence of the decision parameters, i.e. the *FDF* of the hot-spots and the inspection interval Δt_I, on the probabilistic fatigue deterioration process and consequently, on the structural reliability of the system. The employed ID is an extension of the one proposed in Luque and Straub (2019). First, the deterioration model is presented. Second, the relationship between the deterioration model and the system condition is elaborated. Lastly, the likelihood models used for inference of inspection outcomes are described.

Fatigue deterioration model

The structure is subject to a wave-induced cyclic load $\Delta L(t)$ that leads to fatigue stresses in its hot-spots $i = 1, 2, ..., 10$, with long-term distribution ΔS_i represented by a Weibull distribution with scale parameter $k_{\Delta S,i}$ and shape parameter λ_i. As shown in Madsen (1997), the effect of the fatigue stresses on fatigue crack growth can then be captured by the equivalent stress range $\Delta S_{e,i}$, which is defined as:

$$\Delta S_{e,i}(FDF_i) = \mathrm{E}_{\Delta S}[\Delta S_i^{m_i}]^{(1/m_i)} = k_{\Delta S,i}(FDF_i) \cdot \Gamma\left(1 + \frac{m_i}{\lambda_i}\right)^{(1/m_i)} \tag{8}$$

where $\Gamma(\cdot)$ is the gamma function and m_i is a material parameter of the deterioration model, which is modelled according to (Ditlevsen and Madsen 1996). The distributions and values used to represent these parameters are shown in Table 1. Note that $k_{\Delta S,i}$ depends on the fatigue design factor of the hot-spot FDF_i. This relationship is explored further below and shown in Figure 7.

Hot-spots are assumed to contain initial defects, which are represented by an exponential distribution with mean crack length equal to 1 mm. Given this initial crack length, crack growth can then be modelled by a linear elastic fracture mechanics model (LEFM), see Lassen (1997). The stochastic LEFM-based model proposed in Madsen et al. (1987) is used to represent the crack growth model. The crack length at a hot-spot i at time step t is denoted $a_{i,t}$ and given by:

$$a_{i,t} = \left[(1 - m_i/2)C_{i,t}\Delta S_{e,i}^{m_i}\pi^{m_i/2}\nu + a_{i,t-1}^{(1-m_i/2)}\right]^{(1-m_i/2)^{-1}} \tag{9}$$

where ν is the number of stress cycles per time step, $a_{i,t-1}$ is the crack length at the previous time step and C_i is a material parameter. It is assumed that C_i is fully correlated with m_i by the linear model $\ln C_i = -1.567m_i - 27.517$ proposed in Bismut and Straub (2020). The employed values of the basic variables of the fatigue deterioration model are summarized in Table 1. Note that ν is taken as 10^5 cycles/year according to Straub (2009).

The structural reliability of the components is assessed according to the fatigue limit state g_{FM}:

$$g_{FM} = a_{cr} - a_{i,t} \tag{10}$$

where $g_{FM} \leq 0$ represents the event of failure, which happens when the crack length is larger than the critical crack length $a_{cr} = 10$ mm. It is noted that the LEFM-based estimate of fatigue life is rather insensitive to the value of a_{cr}, due to the exponential nature of the model.

The fatigue deterioration process is modelled as a Markov process using the dynamic Bayesian Network (BN) proposed in Straub (2009). This is illustrated in Figure 5, where circular nodes represent random variables, rectangle nodes are decision parameters and the arches represent dependencies, directed from cause to effect. At a given time step t ($0 \leq t \leq T_{SL}$), the crack length of a given hot-spot $a_{i,t}$ is specified conditional on the crack depth at the previous time step $a_{i,t-1}$, and the stochastic crack growth parameters, i.e. the material parameters m_i and C_i, and the scale parameter $k_{\Delta S,i}$ of the Weibull distributed fatigue stress range. Furthermore, if an inspection is conducted ($I_{i,t} = yes$), the inspection outcome $z_{i,t}$ is available. If a repair action is triggered, i.e. $R_{i,t} = yes$, the condition of the hot-spot is set to “as new”.

The correlation and interdependence among components’ deterioration is represented by the hierarchical structure of the BN, as illustrated in Figure 5. The stochastic parameters of the presented deterioration model are explicitly represented by chance nodes, with the exception of C_i, since it is deterministic conditional on m_i. The initial crack length $a_{i,0}$, the material parameter m_i and the stress parameter $k_{\Delta S,i}$ are specified conditional on the hyperparameters α_A, α_M and α_K, respectively. The three hyperparameters are standard normal distributed. The conditional distribution of a deterioration parameter given the hyperparameter is specified so that the joint distribution of the parameter for all hot-spots follows a Gaussian copula with specified correlation coefficients. This hierarchical representation is described in Luque and Straub (2016). The correlation coefficients are set to $\rho_A = 0.5$, $\rho_M = 0.6$ and $\rho_K = 0.8$ for $a_{i,0}$, m_i and $k_{\Delta S,i}$, respectively. Note that the deterioration parameters are conditionally independent for given hyperparameters, which is computationally advantageous to perform Bayesian inference (Luque and Straub 2016). The design decision node $\mathcal{D}$ includes a set of discrete choices of the *FDF* of the hot-spots. Increasing the *FDF* mitigates fatigue by reducing the cyclic stress range. This is represented by the node $\mathcal{D}$ affecting the initial expected scale parameter nodes $k_{\Delta S,i}$ with $i = 1, 2, ..., 10$.

System condition

The system is loaded by a time-variant stochastic load with annual maximum Q, which is represented by a Gumbel distributed random variable with mean value $\mu_Q = 1.05 \cdot 10^6$ N and coefficient of variation 0.35. The value of μ_Q is chosen so that the probability of failure of the undamaged structure is approximately 10^{-6}. The resistance of the system to ultimate load, denoted r, depends on the condition of its members B1-B6 and is assumed to be deterministic.

The dependence between the system condition and the components' deterioration state is modelled with the BN in Figure 6. At a given time step t, the system condition is represented by the node $E_{S,t}$, which has binary outcome space $\{fail, safe\}$. $E_{S,t}$ is specified conditional on the members' condition, denoted $E_{Bj,t}, j = 1, 2, ..., 6$. This is represented by the converging arcs from $E_{Bj,t}$ to $E_{S,t}$. $E_{Bj,t}$ takes the state *safe* if none of the hot-spots of member i is failed and *fail* otherwise. A failed member does not contribute to resistance to ultimate load. Any number of members may fail between two time steps, thus increasing the probability of failure of the system. The deterioration state of the system is characterized by the process $\Psi_t = \{E_{B1,t} \cap E_{B2,t} \cap ... \cap E_{B6,t}\}$, which collects the condition of the members of the system. Note that Ψ_t consists of 2^6 disjoint states that range from all members being safe $\psi_1 = \cap_{j=1}^{6}\{E_{Bj,t} = safe\}$, to all members being failed $\psi_{64} = \cap_{j=1}^{6}\{E_{Bj,t} = fail\}$. The capacity of the system is pre-computed by performing a push-over analysis for all states of Ψ_t, as described in the next subsection. The probability of system failure is computed conditional on Ψ_t as:

$$\Pr(E_{S,t} = fail|\Psi_t = \psi) = \Pr[r(\psi) - Q \leq 0] = 1 - F_Q(r(\psi)) \tag{11}$$

where F_Q is the cumulative distribution function of Q.

The probability of system failure $\Pr(E_{S,t} = fail)$ can then be related to the deterioration state by:

$$\Pr(E_{S,t} = fail) = \int_{\mathbf{a}_t} \sum_{\Psi_t} \Pr(E_{S,t} = fail|\Psi_t)\Pr(\Psi_t|\mathbf{a}_t)\Pr(\mathbf{a}_t)\mathrm{d}\mathbf{a}_t \tag{12}$$

where $\mathbf{a}_t$ is a vector collecting the crack length for all components.

The event of failure of the system up to time t is given by $F_{sys,t} = \{E_{S,1} = fail \cup \ldots \cup E_{S,t} = fail\}$. The cumulative probability of system failure at time t is defined as $\Pr(F_{sys,t})$. This is approximated assuming independence between failure events at different years:

$$\Pr(F_{sys,t}) \approx 1 - \prod_{\tau=1}^{t} \big(1 - \Pr(E_{S,\tau} = fail)\big) \tag{13}$$

It is noted that the error associated with this simplification is reasonably low in this context (Bismut and Straub 2018).

The annual probability of system failure $\Pr(F_{sys,yr,t})$ is simply computed from the cumulative probability of system failure as:

$$\Pr(F_{sys,yr,t}) = \Pr(F_{sys,t}) - \Pr(F_{sys,t-1}) \tag{14}$$

Push-over analysis

A push-over analysis of the structure is performed to determine the ultimate resistance of the system as a function of the configuration of the system $r(\Psi_t)$. This is done using the software USFOS (Søreide et al. 1993). The analysis consists in applying a lateral load as shown in Figure 3, increasing its amplitude until its ultimate resistance is reached. This push-over analysis is performed for all $2^6 = 64$ possible configurations of the system Ψ_t. The employed FE model considers non-linear material behavior, global buckling of the members, large displacements and deformations, formation of plastic hinges and load redistribution within the structural system. Additionally, a limit state of maximum displacement is defined. The maximum allowed displacement at the node where the load is applied is set to 1.5 m.

The nominal dimensions of the tubular members are shown in Table 2. These dimensions are specified at an intermediate cross-section located outside of the area influenced by the welded connection, where stress concentration exists. The single element importance *SEI* is provided in addition as a measure of a member's importance. The SEI_i of a component is equal to that of the member that it belongs to. The SEI_i is defined as the difference between the probability of system failure with only component i failed and the probability of failure of the intact system (Straub and Der Kiureghian 2011). It can be observed that all structural components of the considered structure are of approximately equal importance.

Inspection model

The likelihood of detecting a crack is based on the following probability of detection (PoD) curve:

$$\Pr(Z_t = z | a_{i,t} = a) = PoD(a) = \exp(-a/\xi) \quad \text{if } z = 0 \tag{15}$$

where ξ is the expected minimum detectable crack length. Inspections are visually conducted, with $\xi = 10$ mm.

If a crack is detected, it is assumed that the inspection can provide a measurement of the crack size with an associated Gaussian error. The likelihood function $f_{Z_t|a_t=a}(Z_t|a_t = a)$ used for

Bayesian updating is then defined as:

$$f_{Z_t|a_{i,t}=a}(Z_t|a_{i,t} = a) = (1 - PoD(a)) \cdot \frac{\varphi\left(\dfrac{z-a}{\sigma_\varepsilon}\right)}{1 - \Phi\left(\dfrac{-a}{\sigma_\varepsilon}\right)} \quad \text{for } z > 0 \tag{16}$$

where σ_ε is the measurement error, which is set to 0.1 mm, and $\varphi(\cdot)$ and $\Phi(\cdot)$ are the probability density function and cumulative distribution function of the standard Normal distribution, respectively.

Calibration of the LEFM model to the SN approach

The *FDF* in Eq. (7) is a design parameter that is defined according to the SN approach. The employed deterioration model is based on the LEFM approach. Therefore, in order to use the *FDF* as a design parameter, the employed LEFM model needs to be calibrated to the SN-curve that is used to define the *FDF*. The calibration could be applied through several parameters. In this study, the parameter $k_{\Delta S}$ is chosen. The calibration is performed so that both models estimate the same probability of failure at the end of service life (Bismut and Straub 2020). The procedure for the computation of the probability of failure for the LEFM and the SN approach is elaborated hereafter. The results of the calibration are shown in Figure 7.

LEFM

The crack growth model used in the hierarchical ID is rewritten in terms of the number of cycles n and the initial crack length a_0:

$$a(n) = \left[(1 - m/2)C\Delta S_e^m \pi^{m/2} n + a_0^{(1-m/2)}\right]^{(1-m/2)^{-1}} \tag{17}$$

At the end of service life, the structure is subject to $n = \nu \cdot T_{SL}$ cycles. Using Eq. (10), the associated probability of failure results in:

$$\Pr[g_{FM} \leq 0] = \Pr[a_{cr} - a(n = \nu \cdot T_{SL})] \tag{18}$$

This is computed by crude MCS for different values of $\mathrm{E}[k_{\Delta S}]$, see Figure 7.

SN approach

The fatigue design factor *FDF* is a parameter associated with the deterministic SN failure criterion. The cumulative probability of failure associated with a given *FDF* is calculated so that the expected cumulative damage $\mathrm{E}[\Delta D_i]$ reaches the deterministic failure criterion D at the end of fatigue life $T_{FL} = T_{SL} \cdot FDF$:

$$D(T_{FL}) = 1 = \sum_{i=1}^{\nu \cdot FDF \cdot T_{SL}} \Delta D_i \approx \nu \cdot FDF \cdot T_{SL} \cdot \mathrm{E}\left[\Delta D_i\right] \tag{19}$$

The deterministic fatigue lifetime $1/N_F^D$ is estimated according to the following bi-linear diagram:

$$\frac{1}{N_F^D} = \begin{cases} \dfrac{1}{C_1^D} \Delta S^{m_1} \cdot \left(\dfrac{t_w}{t_{ref}}\right)^{q_t m_1} & \text{for } \Delta S \leq \Delta S_q \\ \dfrac{1}{C_1^D} \Delta S^{m_2} S^{m_1 - m_2} \cdot \left(\dfrac{t_w}{t_{ref}}\right)^{q_t m_2} & \text{for } 0 \leq \Delta S < \Delta S_q \end{cases} \tag{20}$$

with parameters taken according to the D-curve prescribed by the Department of Energy (DoE) of UK (SSC 1996): $m_1 = 3$, $m_2 = 5$, $C_1^D = 1.52 \cdot 10^{12}$, $N_q = 10^7$ cycles, $S_q = 2.48$ MPa, $t_{ref} = 16$ mm and $q_t = 0.30$.

The expected number of cycles to failure is computed according to the mean SN-curve associated with the diagram in Eq. (20) (SSC 1996):

$$\begin{cases} \dfrac{1}{N_F} = \dfrac{1}{C_1} B_s^{m_1} \Delta S^{m_1} \cdot \left(\dfrac{t_w}{t_{ref}}\right)^{q_t m_1} & \text{for } B_s \Delta S \leq \Delta S_q \\ \dfrac{1}{N_F} = \dfrac{1}{C_1} B_s^{m_2} \Delta S^{m_2} \Delta S^{m_1 - m_2} \cdot \left(\dfrac{t_w}{t_{ref}}\right)^{q_t m_2} & \text{for } 0 \leq B_s \Delta S < \Delta S_q \end{cases} \tag{21}$$

where $C_1 = 3.99 \cdot 10^{12}$ and B_s is Log-normal distributed with mean 1 and standard deviation 0.25.

Noting that ΔS is Weibull distributed, the expected damage per cycle $\mathrm{E}[\Delta D_i]$ can be expressed as:

$$\mathrm{E}\left[\Delta D_i\right] = \mathrm{E}\left[\frac{1}{N_F}\right] = k^{m_1} \cdot \left(\frac{t_w}{t_{ref}}\right)^{q_t m_1} \cdot \frac{1}{C_1} \cdot \Gamma\left(1 + \frac{m_1}{\lambda}, \left(\frac{\Delta S_q}{k}\right)^{\lambda}\right) + k^{m_2} \cdot \left(\frac{t_w}{t_{ref}}\right)^{q_t m_2} \cdot \frac{1}{C_1} \cdot \Delta S_q^{m_1 - m_2}\left[1 - \Gamma\left(1 + \frac{m_2}{\lambda}, \left(\frac{\Delta S_q}{k}\right)^{k}\right)\right] \tag{22}$$

where $\Gamma(\cdot, \cdot)$ is the incomplete gamma function and λ and k are the shape and scale parameters of the Weibull distribution.

The shape parameter k is calibrated so that Eq. (19) is satisfied. The cumulative probability of failure for a duration of T_{SL} years is computed as $\Pr[g_{SN} \leq 0]$, with g_{SN} being the SN-approach limit state function:

$$g_{SN} = \Delta - \nu \cdot T_{SL} \cdot \mathrm{E}\left[\Delta D_i\right] \tag{23}$$

Note that Δ is a Log-normal random variable with mean 1 and standard deviation 0.3 that represents the uncertainty associated with the Palmgren-Miner failure criterion (JCSS 2001).

The probability of failure $\Pr[g_{SN} \leq 0]$ is computed for different values of the *FDF* using first order reliability method (FORM), see Figure 7.

Calibration

The mean value of $k_{\Delta S}$ used in the LEFM deterioration model is calibrated to the SN approach as a function of the *FDF* by ensuring that both models estimate the same probability of failure at the end of service life. The relationship between $\mathrm{E}[k_{\Delta S}]$ and the *FDF* is shown in Figure 7.

Cost model

The IMF cost $C_{IMF}(\mathcal{S}_i, \mathcal{D}_j)$ is defined in Eq. (3) as the sum of the discounted costs of campaign, inspection, repair and failure. These costs are calculated based on the cost input in Table 3. These costs are rough estimates based on the cost of inspection given in Salmon, J. (2015) and the cost ratios in Luque and Straub (2019). An annual discount rate $i_r = 0.02$ is used.

The cost associated with a certain design choice C_D needs to be coherent with the aforementioned cost function. A design choice comprises the specification of the *FDF* for the different hot-spots. The relation between the *FDF* and the fatigue stress is established through $E[k_{\Delta S}]$, see Figure 7.

The fatigue stress range ΔS can be linked to a certain cross-section area, given that the cycling loading is known. Given that the fatigue stress is of a predominantly axial nature, i.e. the stress associated with bending and shear forces can be neglected, the relationship between $\Delta S_i(t)$ and the required cross-section area of the tubular member at the connection $A_{HS,i}$ is given by:

$$\Delta S_i(t) = \frac{\Delta N_i(t)}{A_{HS,i}} \tag{24}$$

where subscript i refers to the hot-spot i, $\Delta N_i(t)$ is the nominal cyclic axial force range. Note that the cross-section area $A_{HS,i}$ is specified within the region affected by the stress concentration due to the tubular joint of interest and it is typically different than the nominal area specified at an intermediate cross-section by the dimensions in Table 2.

A linear relation between the fatigue load $\Delta L(t)$ and the internal forces at a member $\Delta N_i(t)$ can be established given that linear elasticity theory is applicable. In that case, it suffices to calculate $\Delta N_i(t)$ for one value of $\Delta L(t)$. The axial forces associated with a unitary load, i.e. $\Delta L = 1$, here called α_{Bi}, are plotted in Figure 8. The internal forces can be computed simply as $\Delta N_i(t) = \alpha_{Bi} \cdot \Delta L(t)$, for any value of the fatigue loading.

The area $A_{HS,i}$ of hot-spot i can then be expressed as a function of the mean equivalent fatigue stress range at year zero $\mathrm{E}[\Delta S_{e,i}]$ and the equivalent fatigue load range ΔL_e:

$$\begin{aligned} A_{HS,i}(FDF_i) &= \frac{|\alpha_{Bj}| \cdot \Delta L_e}{\mathrm{E}[\Delta S_{e,i}]} = \\ &= \frac{|\alpha_{Bj}| \cdot \Delta L_e}{\mathrm{E}[k_{\Delta S,i}](FDF_i) \cdot \mathrm{E}\left[\Gamma\left(1 + \frac{m_i}{\lambda}\right)^{(1/m_i)}\right]} \end{aligned} \tag{25}$$

where j refers to the member associated with hot-spot i and $\Delta L_e = \mathrm{E}[\Delta L^m]^{(1/m)}$ is assumed to be 600 kN. Note that Eq. (8) is used to express $\Delta S_{e,i}$ as a function of $k_{\Delta S,i}$ and that the relationship between $\mathrm{E}[k_{\Delta S}]$ and FDF is shown in Figure 7.

By using Eq. (25), the cross-section area of the tubular member at the connection $A_{HS,i}$ can be expressed as a function of FDF_i. $A_{HS,i}$ is plotted as a function of the FDF for the different members in Figure 9.

The cost of fatigue design of a single hot-spot $C_{HS,i}$ is defined as:

$$C_{HS,i}(FDF_i) = \rho_s \cdot c_s \cdot A_{HS,i}(FDF_i) \cdot 1.5 d_{o,i} \tag{26}$$

where ρ_s is the steel density, here assumed to be 7850 kg/m^3. c_S is the cost of steel per unit weight, which is around 2-3€/kg (De Vries et al. 2011). In this case study, c_S is assumed to include the cost of welding and it is set to 6€/kg. The last term of the expression, i.e. $1.5d_{o,i}$, refers to the extension of the tubular joint, with $d_{o,i}$ being the outer diameter of the tubular member at the joint. Thus, $A_{HS,i} \cdot 1.5d_{o,i}$ is an estimation of the volume of steel employed in the fabrication of the tubular connection. A large number of combinations of diameter d_o and thickness t_w could be used in practice to achieve the same area $A_{HS,i}$. The ratio $k_{dt} = d_o/t_w$ is introduced. The cross-section area $A_{HS,i}$ can be expressed as a function of $d_{o,i}$ and $t_{w,i}$ by use of the simplified formula $A_{HS,i} = \pi(d_{o,i} - t_{w,i}) \cdot t_{w,i}$. It is straightforward then to express the diameter as a function of the cross-section area and k_{dt}:

$$d_{o,i} = \sqrt{\frac{A_{HS,i} \cdot k_{dt}}{\pi\,(1 - 1/k_{dt})}} \tag{27}$$

A typical range of k_{dt} for tubular members of offshore lattice structures is 10 to 50. The cost of fatigue design $C_{HS,i}$ is calculated for this range of k_{dt} and plotted in Figure 10. Only the cost of B1 and B3 is plotted for clarity of the figure. The mean value, which is highlighted by a dashed line in the plot, is used for the cost model of the case study. The cost of fatigue design C_D is computed as the sum of $C_{HS,i}$ for all hot-spots $i = 1, 2, ..., 10$.

Discretization for the BN model

The discretization of the random variables in the BN is performed according to recommendations in Straub (2009). According to Luque and Straub (2016), one state is sufficient to represent the failure domain of the deterioration variable, i.e. any realization $a_t \geq a_c$ is represented by one single state that ranges between a_c to infinity. However, this introduces an error in the smoothing operation performed in the employed algorithm for Bayesian inference (Zhu and Collette 2015).

The discretization selected in this study takes these considerations into account and provides a good enough trade off between computation time and accuracy.

RESULTS OF THE CASE STUDY

Three designs $\mathcal{D}$ are tested as shown in Table 4. Since the importance of the hot-spots is similar, as shown in Table 2, all the dry hot-spots (HS1-HS4) are assigned the same FDF, denoted FDF_d and all submerged hot-spots (H5-H10) are assigned the same the same FDF, denoted FDF_s. The effect of varying FDF_d is studied. FDF_s is kept constant and equal to 6 for all designs for simplicity.

As mentioned above, the aim of this framework is not to assess optimal I&M strategies but to enhance the design decisions. With this in mind, the optimization of I&M strategies is limited to the optimization within a discrete set of inspection intervals Δt_I. Inspections of all dry hot-spots every two, five and ten years are considered, plus the case in which no inspections are performed. Furthermore, a decision rule is applied: any detected damage is assumed to be repaired and thereby restored to the initial condition.

Effect of correlation

An important benefit of considering system effects is that the dependency among hot-spots' deterioration is explicitly taken into account. Consequently, information obtained by inspecting a certain hot-spot is used to update the belief on the deterioration state at other correlated hot-spots. The effect of correlation among the deterioration processes at different hot-spots can be observed in Figure 11. The time evolution of the cumulative probability of failure of hot-spots HS1 and HS5 is plotted. In this example, HS1 is inspected every five years without detecting any crack. HS5, which belongs to B4 and is located underwater, cannot be inspected. These results are given for Design 3, with $FDF_d = FDF_s = 6$. Therefore, the prior probability of failure is equal for both hot-spots. It can be seen that inspecting HS1 and not finding a crack decreases the estimated probability of system failure of HS5 through the statistical dependence among the fatigue processes.

Effect of *FDF* on the probability of system failure

The time evolution of the posterior annual probability of failure of the system is compared for the three considered designs in Figure 12. Δt_I is set to five years, which means that three inspections are carried out at years 5, 10 and 15. Note that at year t, the annual probability of system failure $\Pr(F_{sys,yr})$ is estimated by Monte Carlo simulation over the observation outcomes up to that time.

It can be observed that the *FDF* has a significant impact on the time-variant system reliability, which is strongly affected by the speed of the hot-spot deterioration, i.e. the growth rate $\mathrm{d}a(t)/\mathrm{d}n(t)$, which is proportional to the fatigue stress range to the m-th power and consequently inversely proportional to the *FDF*. Thus, doubling the *FDF* decreases the crack growth rate by about 50%. Unfortunately, due to the complexity of the system, it is not possible to establish a simple relationship between $\Delta S(t)^m$ and the probability of system failure. In general, the effect of increasing the *FDF* will be larger when the probability of system failure is larger. Therefore, the reduction achieved by increasing the *FDF* from 2 to 4 will be larger than that from 4 to 6. For $\Delta t_I = 2$ yr, increasing FDF_d from 2 to 4 and from 4 to 6, reduces the probability of system failure at the end of service life by 51% and 46%, respectively. For the same reason, the reduction will be larger when no inspections are conducted. In that case, 83% reduction of the probability of failure is achieved by increasing FDF_d from 2 to 4 and 67% by increasing FDF_d from 4 to 6.

Effect of I&M on the probability of system failure

The time evolution of the annual probability of failure of the system $\Pr(F_{sys,yr})$, including sampled observation histories, is plotted for different inspection strategies $\mathcal{S}$ in Figure 13 for Design 1. It can be seen that the frequency of I&M campaigns has a clear effect on the annual reliability, helping to mitigate the annual risk in between inspections.

Expected life-cycle cost and optimal design

Figure 14 shows the expected life-cycle cost for the different considered designs $\mathcal{D}$ and I&M strategies $\mathcal{S}$. The optimal I&M strategies for designs 1, 2 and 3 are two, five and ten years, respectively. The optimal integrated design, which is defined according to Eq. (1), is found to be $\{\mathcal{D}_{opt}, \mathcal{S}_{opt}\} = \{\text{Design } 3, \Delta t_I = 10 \text{ years}\}$. It can be observed that, for the given cost model, it is cost-efficient to invest in a more conservative design. This initial investment in the construction of the structural details is compensated by a reduced expected investment in inspections and repairs. It can also be seen that allowing for a slightly larger risk and inspecting every ten years instead of five is cost-effective.

The *FDF* has a clear effect on the expected consequences of failure. In particular, the effect is easily appreciated for the cases with no inspections, where the expected cost is dominated by the risk of failure, particularly for smaller values of the *FDF*. For $FDF_d = 2$, the expected life-cycle cost associated with no inspections is disproportionate compared to the cases with inspections, being approximately 11 times larger than for $\Delta t_I = 2$ years. The importance of the *FDF* is less evident when an intensive inspection control is performed, such as for $\Delta t_I = 2$ years, where the expected life-cycle cost is approximately the same for all the tested designs. In general, it is observed that increasing the *FDF* shifts the optimal I&M policies towards longer inspection intervals.

Influence of the annual discount rate

The estimation of the expected life-cycle cost $\mathrm{E}[C_T]$ is sensitive to the annual discount rate i_r. Typical values of the annual discount rate range between 0.02 and 0.05. In order to study the influence of the annual discount rate on optimal life-cycle decisions, the expected life-cycle cost is plotted for these two values as a function of the inspection interval Δt_I and for the three designs in Figure 15. It can be observed that increasing i_r from 0.02 to 0.05 leads to a significant reduction of $\mathrm{E}[C_T]$. This reduction mainly concerns the risk of failure term. For the case of no inspections and $FDF_d = 2$, the risk of failure decreases by approximately 40%. Fortunately, the optimal choice of an inspection interval is more robust with regard to changes of this parameter. For this particular case study, the optimal I&M planning given each of the three design specifications remains the same for both values of the annual discount rate.

Accuracy of the Monte Carlo estimate

In the present study, $n_{sim} = 350$ sampled histories are used to estimate the expected life-cycle cost for each tested design and strategy. The coefficient of variation $\hat{\nu}_{\mathrm{E}_Z[C_T]}$ is introduced to assess the accuracy of the estimation of the expected life-cycle cost:

$$\hat{\nu}_{\mathrm{E}[C_T]} = \frac{1}{\sqrt{n_{sim}}} \cdot \frac{\sqrt{\mathrm{Var}_Z[C_T(\mathcal{S}_i, \mathcal{D}_j|\mathbf{Z})]}}{\mathrm{E}_Z[C_T(\mathcal{S}_i, \mathcal{D}_j|\mathbf{Z})]} \tag{28}$$

where $\mathrm{Var}_Z[\cdot]$ is the variance operator upon the set of observations Z.

For designs 1, 2 and 3, respectively, it results in $\hat{\nu}_{\mathrm{E}[C_T]} = \{0.087, 0.080, 0.013\}$ for $\Delta t_I = 2$ yr, and $\hat{\nu}_{\mathrm{E}[C_T]} = \{0.080, 0.076, 0.035\}$ for $\Delta t_I = 5$ yr. It is seen that the estimation of $\mathrm{E}[C_T]$ is associated with relatively large uncertainties. Nonetheless, this accuracy is sufficient to compare the effect of the different I&M strategies and to assess the optimal integrated design for the explored decision alternatives.

DISCUSSION

The presented framework can be used to assess a cost-effective balance between the design investments and expected I&M costs and inform about the efficiency of the safety measures. The paper focuses on fatigue deterioration, but the framework can be applied to other phenomena, such as corrosion. Moreover, information about the importance of the components regarding system structural integrity, the components dependency and the inspectability of a structural detail can be efficiently utilized for the identification of optimal design decisions.

The framework only considers decisions related to structural deterioration in order to keep the model as simple as possible. Therefore, not all aspects that a structural design should consider are contemplated in the model. Nevertheless, it is expected that I&M planning decisions will mainly influence the design decisions related to deterioration. Additional limit states could be added ad-hoc into the model. For instance, serviceability limit states such as maximum allowed deflection, could be added as a design constraint. Alternatively, additional limit states could be taken into account in a prior assessment of the design.

Another limitation of the model is its computational demand. Although it increases linearly with the number of hot-spots, the increase is exponential with the amount of random variables (Luque and Straub 2016). The computational demand also increases dramatically with the number of inspection campaigns. Using an Intel Xeon Gold 6132 processor, the computational time per sampled history grows from ca. 22 s when no inspections are conducted to ca. 230 s for $\Delta t_I = 2$ years. Additionally, 2^N push-over analysis (with N being the number of structural elements that contain fatigue prone details) are to be performed prior to the generation of the BN in order to estimate the reliability of the damaged system. This becomes intractable for relatively small systems. For 12 structural elements, 4096 analysis are to be performed. Assuming that a push-over analysis takes in average 20 s, this requires ca. 22 h. For 14 elements, which is still a small number of components for e.g. an offshore jacket structure, the push-over analysis requires approximately 4 days. Therefore, for structures with more than say 12 components, a smart selection of the cases is to be performed beforehand. This could be done by identifying for which cases the structure is structurally under-determinate or by ranking the elements based on their contribution to the probability of system failure (Luque and Straub 2016; Kim et al. 2013).

Further research

The proposed framework can be used to assess the optimal trade-off between investments in design and I&M for a particular structure or portfolio of structures. Unfortunately, identified optimal decisions may not ensure a sufficient safety level from a societal point of view. The marginal life-saving cost principle together with the life-quality index can be used to assess if risk can be further mitigated in a cost-effective way according to societal preferences (Nathwani et al. 1997). This assessment should be conducted considering all reasonable mitigation measures.

There are challenges associated with the implementation and dissemination of the proposed model. Currently, applying the framework to systems with a large number of deteriorating components or using deterioration models with more stochastic parameters than the one used in this paper is computationally unfeasible. Moreover, due to the complexity of the model, building the model and interpreting the results require of expert knowledge. Nevertheless, the insight that can be gained from it could be summarized as prescription rules and requirements for reliability-based design. Standards such as ISO (2015) prescribe acceptable safety levels according to the consequence class and the relative costs of the safety measures. The proposed framework can be used to extend the differentiation of prescribed safety level to consider the level of inspectability of a structural detail. In addition, the proposed framework can be used to find the optimal safety level at the design stage given the characteristics of the system, the relative cost of safety measures and a consequence class.

CONCLUSIONS

A risk-based decision framework for the design of large infrastructure systems was presented in this paper. The proposed framework presents an enhanced formulation of the design decision problem in which design decisions can be made taking aspects of inspection planning into account. The framework focuses on fatigue design and the optimal allocation of resources to mitigate risk of fatigue failure. The framework considers system effects. This has an impact on the quantification of the reliability of the structure and the optimization of the mitigation measures.

The methodology was implemented to a simple example, an offshore lattice structure subject to fatigue deterioration. Considered mitigation measures are the specification of the fatigue design factors of the hot-spots as well as the time interval between inspections and possible repair. Inspections were assumed imperfect and therefore their outcome was associated with uncertainty. Furthermore, not all hot-spots were considered to be accessible. The example showed the feasibility of the methodology and documented the challenges in its implementation. Results show a significant influence of the periodicity of inspections and the fatigue design of components on the life-cycle risk. It is seen that optimal fatigue design is enhanced by the consideration of life-cycle risk mitigation measures.

DATA AVAILABILITY STATEMENT

Some or all data, models, or code that support the findings of this study are available from the corresponding author upon reasonable request. This includes the push-over analysis data and the code used for conducting the integrated design optimization.

ACKNOWLEDGEMENTS

The COST Action TU1402 on Quantifying the Value of Structural Health Monitoring is gratefully acknowledged for enabling the research collaboration through an STSM grant. This work was also supported by Deutsche Forschungsgemeinschaft (DFG) through the TUM International Graduate School of Science and Engineering (IGSSE).

REFERENCES

A. Almar-Næss, ed. (1985). *Fatigue handbook : offshore steel structures*. Tapir, Trondheim.

API (2002). “Recommended practice for planning, designing and constructing fixed offshore platforms—working stress design.” *API RP 2A-WSD*, API Publishing Services, Washington, D.C, USA.

Athenosy, L., Omic, E., and Halb, J. (2017). “Investing in Public Infrastructure in Europe.” *Report no.*, Council of Europe Development Bank. `https://coebank.org/media/documents/Investing_in_Public_Infrastructure_in_Europe_27dc1Pg.pdf`.

Bismut, E. and Straub, D. (2018). “Adaptive Direct Policy Search for Inspection and Maintenance Planning in Structural Systems.” *International Symposium on Life-Cycle Civil Engineering IALCCE 2018*, Ghent.

Bismut, E. and Straub, D. (2020). “Optimal adaptive inspection and maintenance planning for deteriorating structural systems.” *Reliability Engineering & System Safety* Under review.

BSI (2015). “Guide to fatigue design and assessment of steel products.” *BS 7608:2014+A1:2015*, BSI Group.

CEN (2005). “Eurocode 3: Design of steel structures part 1-9: Fatigue.” *EN 1993-1-9:2005: E*, CEN, Brussels, Belgium.

Cramer, E. H. and Friis-Hansen, P. (1994). “Reliability-based optimization of multi-component welded structures.” *Journal of offshore mechanics and Arctic engineering*, 116(4), 233–238.

De Vries, W. E., Vemula, N. K., Passon, P., Fischer, T., Kaufer, D., Matha, D., Schmidt, B., and Vorpahl, F. (2011). “Final report WP 4.2: support structure concepts for deep water sites: deliverable D4.2.8.” *Report No. 019945*, WP4: offshore foundations and support structures.

Ditlevsen, O. and Madsen, H. O. (1996). *Structural reliability methods*, Vol. 178. Wiley New York, Copenhagen, Denmark.

DNV-GL (2015). “Probabilistic methods for planning of inspection for fatigue cracks in offshore structures.” *DNVGL-RP-C210*, DNV-GL.

DNV-GL (2016). “Fatigue design of offshore steel structures.” *DNVGL-RP-C203*, DNV-GL.

Faber, M. H., Engelund, S., Sørensen, J. D., and Bloch, A. (2000). “Simplified and generic risk based inspection planning.” *Simplified and Generic Risk Based Inspection Planning*.

Faber, M. H., Sørensen, J. D., Tychsen, J., and Straub, D. (2005). “Field implementation of rbi for jacket structures.” *Journal of Offshore Mechanics and Arctic Engineering*, 127(3), 220–226.

FHWA (2020). “National bridge inventory.” *U.S. Department of Transportation, Federal Highway Administration*. https://www.fhwa.dot.gov/bridge/nbi/ascii.cfm [Accessed: 2020-02-05].

Garbatov, Y., Sisci, F., and Ventura, M. (2018). “Risk-based framework for ship and structural design accounting for maintenance planning.” *Ocean Engineering*, 166, 12 – 25.

Gintautas, T., Sørensen, J. D., et al. (2018). “Reliability-based inspection planning of 20 mw offshore wind turbine jacket.” *International Journal of Offshore and Polar Engineering*, 28(03), 272–279.

Gurney, T. R. (1979). *Fatigue of welded structures*. CUP Archive.

Hobbacher, A. F. (2016). “Recommendations for Fatigue Design of Welded Joints and Components.” *IIW-2259-15*, Springer International Publishing.

HSE (1995). “Guidance on design, construction and certification.” *Offshore Installations*, HSE Books, Merseyside, United Kingdom, 4 edition.

HSE (2001). “Comparison of fatigue provisionsin codes and standards.” *techreport*, Health and Safety Executive. Offshore technology report 2001/083.

ISO (2007). “Petroleum and natural gas industries — Fixed steel offshore structures.” *ISO 19902:2007*, pub-ISO, Geneva, Switzerland.

ISO (2015). “General principles on reliability for structures.” *ISO 2394:2015*, pub-ISO, Geneva, Switzerland.

JCSS (2001). “Part 3: Resistance models.” *Probabilistic Model Code*, Joint Committee on Structural

Safety.

Kalaitzidakisa, P. and Kalyvitisb, S. (2005). “Financing ‘new’ public investment and/or maintenance in public capital for growth?.” *Economic Inquiry*, 43, 586–600.

Kim, D.-S., Ok, S.-Y., Song, J., and Koh, H.-M. (2013). “System reliability analysis using dominant failure modes identified by selective searching technique.” *Reliability Engineering & System Safety*, 119, 316–331.

Lassen, T. (1997). “Experimental investigation and stochastic modelling of the fatigue behaviour of welded steel joints.” Ph.D. thesis, Dept. of Building Technology and Structural Engineering, Aalborg University, University of Aalborg.

Lincoln, J. W. (1985). “Damage Tolerance–USAF Experience.” *Proceedings of the 13th Symposium of the International Committee on Aeronautical Fatigue, Pisa, Italy*, Vol. 131.

Luque, J. and Straub, D. (2016). “Reliability analysis and updating of deteriorating systems with dynamic Bayesian networks.” *Structural Safety*, 62, 34–46.

Luque, J. and Straub, D. (2019). “Risk-based optimal inspection strategies for structural systems using dynamic Bayesian networks.” *Structural Safety*, 76, 68–80.

Madsen, H., Skjong, R., and Tallin, A. (1987). “Probabilistic fatigue crack growth analysis of offshore structures, with reliability updating through inspection.” *Marine Structural Reliability Engineering Symposium*.

Madsen, H. and Sorensen, J. (1990). “Probability-based optimization of fatigue design, inspection and maintenance.” *Proceedings of the Integrity of Offshore Structures*.

Madsen, H. O. (1997). “Stochastic modeling of fatigue crack growth and inspection.” *Probabilistic methods for structural design*, Springer, 59–83.

Márquez-Domínguez, S. and Sørensen, J. D. (2012). “Fatigue reliability and calibration of fatigue design factors for offshore wind turbines.” *Energies*, 5(6), 1816–1834.

McAuliffe, F. D., Murphy, J., Lynch, K., Desmond, C., Norbeck, J. A., Nonås, L. M., Attari, Y., Doherty, P., Sorensen, J. D., and Giebhardt, J. (2017). “Driving Cost Reductions in Offshore Wind.” *Report no.*, Leanwind. `http://www.leanwind.eu/wp-content/uploads/`

LEANWIND-final-publication.pdf.

Moan, T. (2018). "Life cycle structural integrity management of offshore structures." *Structure and Infrastructure Engineering*, 14(7), 911–927.

Moan, T., Hovde, G., Blanker, A., et al. (1993). "Reliability-based fatigue design criteria for offshore structures considering the effect of inspection and repair." *Offshore Technology Conference*, Offshore Technology Conference.

Nathwani, J. S., Lind, N. C., and Pandey, M. D. (1997). "Affordable safety by choice: the life quality method." *Institute for risk research*, 245, 1997.

NORSOK (2004). "Design of steel structures." *N-004*, Standards Norway., Lysaker, Norway.

Rioja, F. (2013). "What is the value of Infrastructure Maintenance? A Survey." *Infrastructure and Land Policies*, 13, 347–365.

Salmon, J. (2015). "Choosing the right blade maintenance regime." *Wind Power Monthly*. http://www.windpowermonthly.com/article/1369612/choosing-right-blade-maintenance-regime [Accessed: 2019-03-08].

Shirley, Chad (2017). "Spending on infrastructure and investment." *Congresional Budget Office*. https://www.cbo.gov/publication/52463 [Accessed: 2019-05-31].

Sørensen, J. D. (2011). "Reliability-based calibration of fatigue safety factors for offshore wind turbines." *The Twenty-first International Offshore and Polar Engineering Conference*, International Society of Offshore and Polar Engineers.

SSC (1996). "Probability based ship design: Implementation of design guidelines: a demonstration." *techreport Report #392*, Ship Structure Committee.

Straub, D. (2004). "Generic approaches to risk based inspection planning for steel structures." Ph.D. thesis, Swiss Federal Institute of Technology Zürich, Zürich, Switzerland.

Straub, D. (2009). "Stochastic modeling of deterioration processes through dynamic Bayesian networks." *Journal of Engineering Mechanics*, 135(10), 1089–1099.

Straub, D. and Der Kiureghian, A. (2011). "Reliability acceptance criteria for deteriorating elements of structural systems." *Journal of Structural Engineering*, 137(12), 1573–1582.

Straub, D., Goyet, J., Sørensen, J. D., and Faber, M. H. (2006). "Benefits of risk based inspection planning for offshore structures." *25th International Conference on Offshore Mechanics and Arctic Engineering*, American Society of Mechanical Engineers, 59–68.

Søreide, T. H., Amdahl, J., Eberg, E., et al. (1993). "USFOS - a computer program for progressive collapse analysis of steel offshore structures. theory manual." *techreport*, SINTEF, Trondheim, Norway.

Zhu, J. and Collette, M. (2015). "A dynamic discretization method for reliability inference in dynamic bayesian networks." *Reliability Engineering & System Safety*, 138, 242 – 252.

Zou, G., Banisoleiman, K., González, A., and Faber, M. H. (2018). "A probabilistic approach for joint optimization of fatigue design, inspection and maintenance." *The Twenty-eighth (2018) International Ocean and Polar Engineering Conference, Sapporo, Japan, 10-15 June 2018*.

List of Tables

TABLE 1. Mean value μ and standard deviation σ of the variables of the deterioration model used in the case study.

Variable	Type	μ	σ
$a_{i,0}$	Exponential	1 mm	1 mm
m_i	Normal	3.5	0.3
$k_{\Delta S,i}$	Log-normal	$f(FDF_i)$	0.22 N/mm^2
λ_i	Deterministic	0.8	-
a_{cr}	Deterministic	10 mm	-
ν	Deterministic	10^5 cycles/year	-
T_{SL}	Deterministic	20 years	-

TABLE 2. Characteristics of the six tubular members. Nominal cross-section dimensions are given by the outer diameter d_0 and the wall thickness t_w. SEI_i refers to the single element importance of the member i.

Member i	d_o [m]	t_w [m]	SEI_i
B1, B2	0.480	0.009	2.90 E-03
B3, B4	0.520	0.010	5.26 E-03
B5, B6	0.520	0.010	2.60 E-03

TABLE 3. Cost input.

Cost	Symbol	Value
Inspection campaign	c_C	1 k€
Component inspection	c_I	0.3 k€
Component repair	c_R	0.6 k€
System failure	c_F	3,000 k€
Cost of steel	c_S	6 € /kg

TABLE 4. Fatigue design factor *FDF* for the three tested designs. FDF_d and FDF_s refer to the *FDF* of the inspectable and non-inspectable hot-spots, respectively.

$\mathcal{D}$	Design 1	Design 2	Design 3
FDF_d	2	4	6
FDF_s	6	6	6

List of Figures

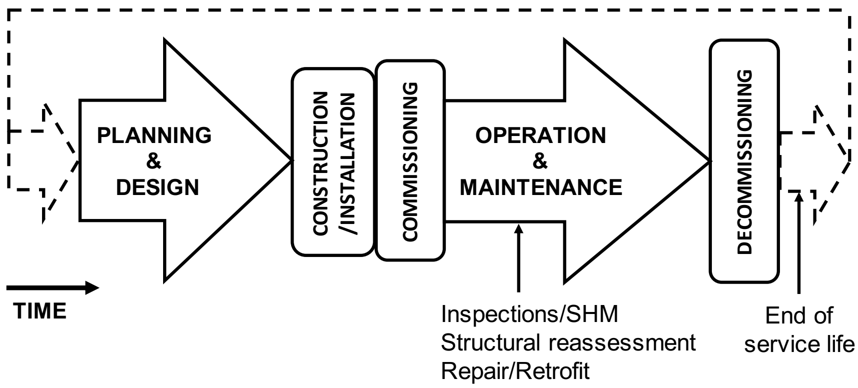

Fig. 1. Main phases of the life-cycle of large structural systems.

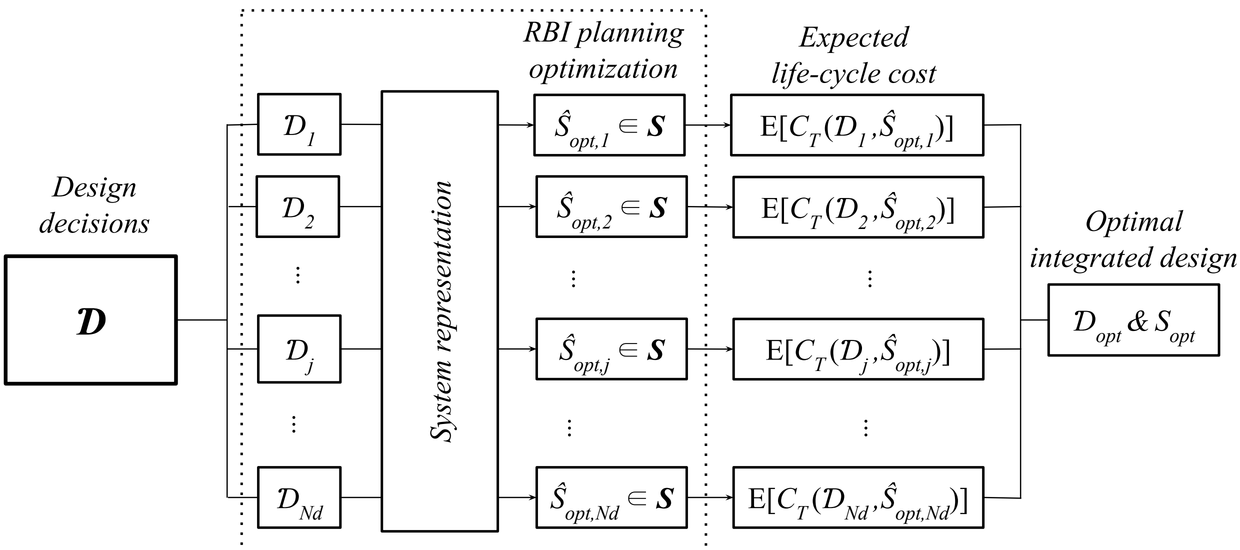

Notes: N_d = number of considered designs; $\boldsymbol{S}$ = considered I&M strategies; $\hat{S}_{opt,j}$ = optimal I&M strategy given design $\mathcal{D}_j$, RBI planning = risk-based inspection planning

Fig. 2. Schematic representation of the integrated structural design framework.

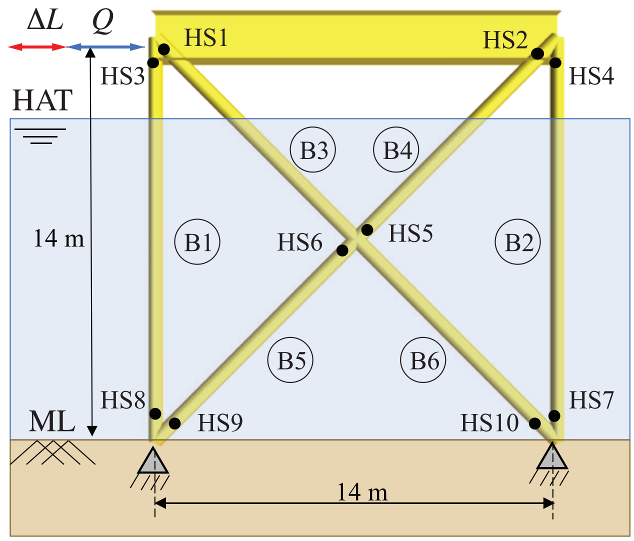

Fig. 3. Case study structure: offshore lattice structure subject to fatigue deterioration at ten hot-spots (HS1-HS10) that are located at the welded tubular joints of the braces B1-B6.

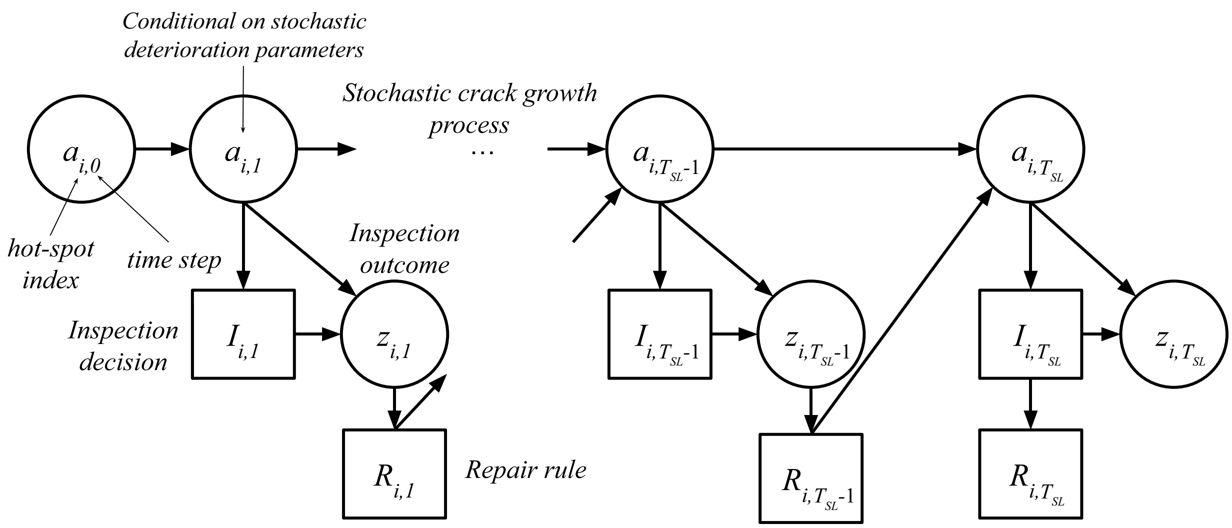

Fig. 4. Schematic influence diagram of the fatigue deterioration model. The crack length of a hot-spot i at year t, denoted $a_{i,t}$, is specified conditional on the stochastic deterioration parameters and evolves in time according to Eq. (9).

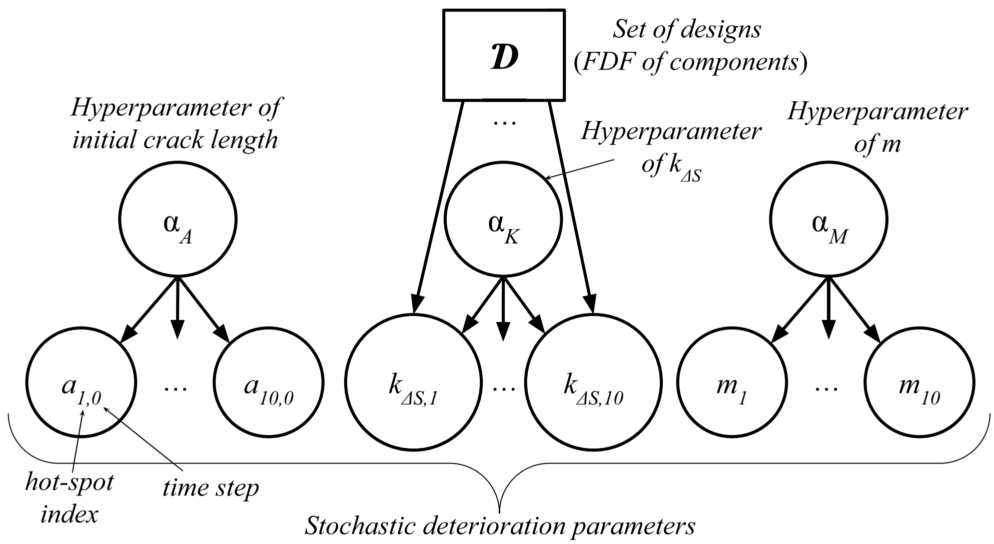

Fig. 5. Dependence structure of the fatigue deterioration process modelled through the correlation of the stochastic deterioration parameters $a_{i,0}$, $k_{\Delta S,i}$ and m_i among different hot-spots $i = 1, 2, \ldots, 10$ with a hierarchical Bayesian Network.

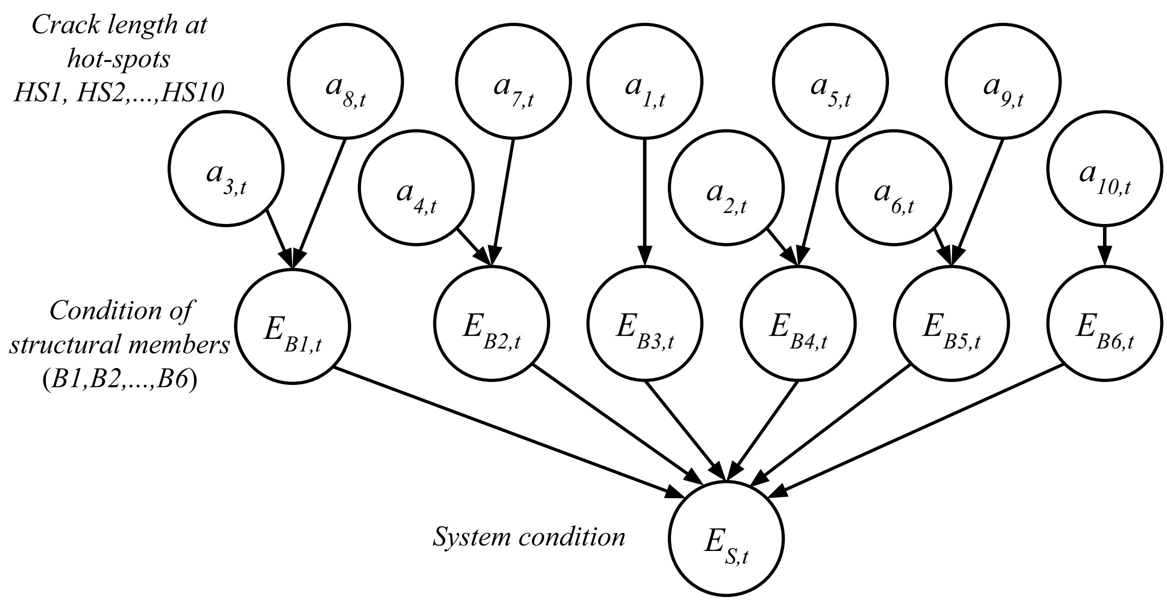

Fig. 6. Bayesian Network model of the relationship between the crack length of the hot-spots, the condition of the structural members and the system condition at time step t.

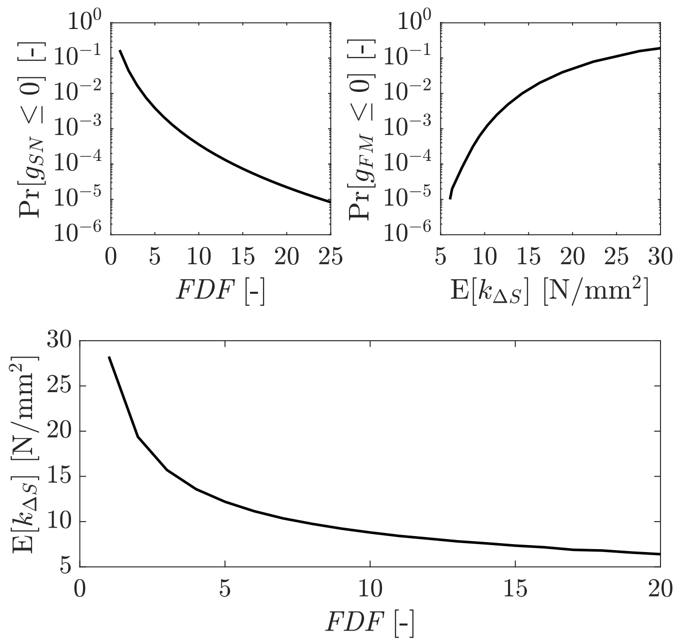

Fig. 7. Calibration of the mean value of the stochastic scale parameter $k_{\Delta S}$ of the Weibull distributed fatigue stress range process as a function of the fatigue design factor *FDF*, so that the fracture mechanics and the SN approaches result in the same probability of failure at the end of service life.

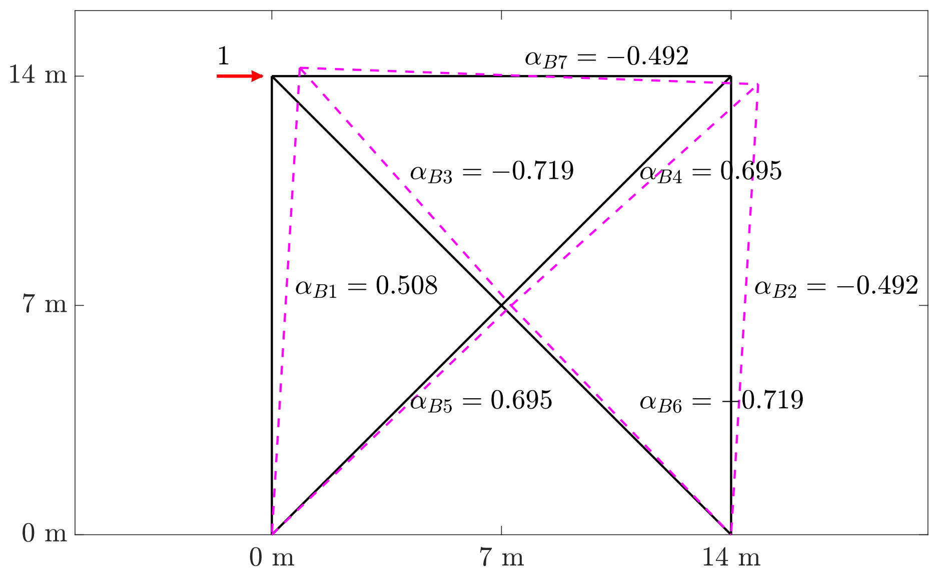

Fig. 8. Axial forces in the members for a unit load.

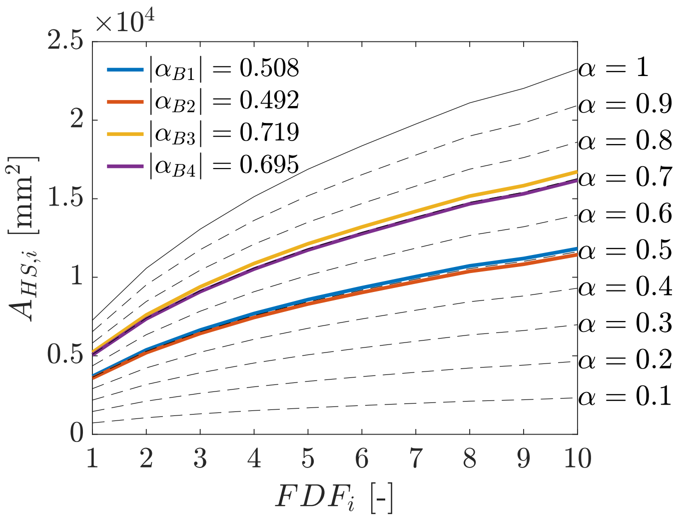

Fig. 9. Cross-section area of a joint $A_{HS,i}$ as a function of the fatigue design factor *FDF* plotted for the members B1-B4 and for different values of α.

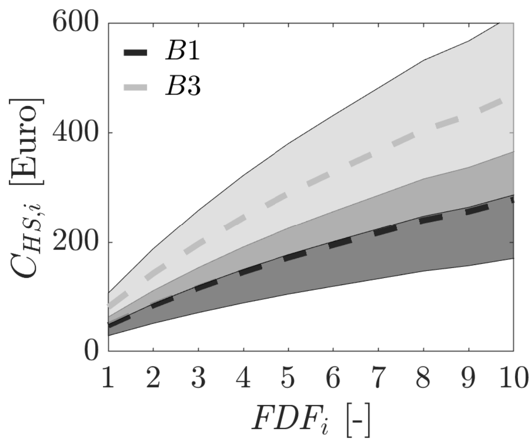

Fig. 10. Design cost of a hot-spot $C_{HS,i}$ as a function of the fatigue design factor *FDF* for the members B1 and B3. The colored areas referred to values of the diameter to thickness ratio in the range from 10 to 50 and the dashed lines are the mean values within that range.

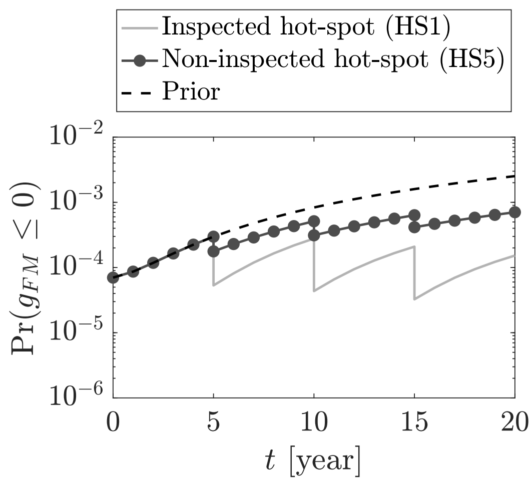

Fig. 11. Posterior cumulative probability of failure $\Pr(g_{FM} \leq 0)$ of inspected hot-spot HS1 and non-inspected hot-spot HS5. In this example, inspected hot-spots are associated with $FDF_d = 6$ and inspected every five years with no crack detection at any instance.

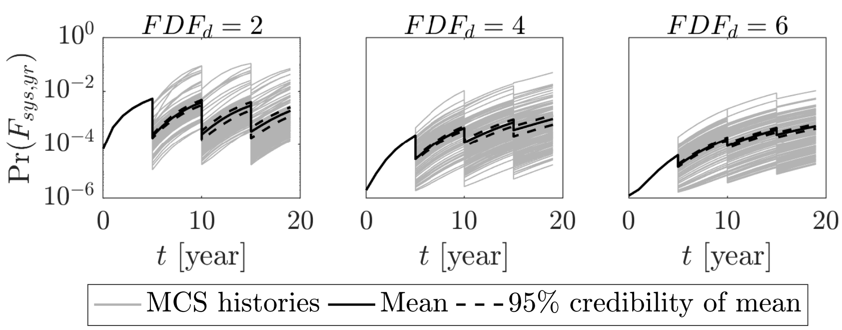

Fig. 12. Comparison of the annual probability of system failure of $\Pr(F_{sys,yr})$ between the three tested designs, with $\Delta t_I = 5$ yr.

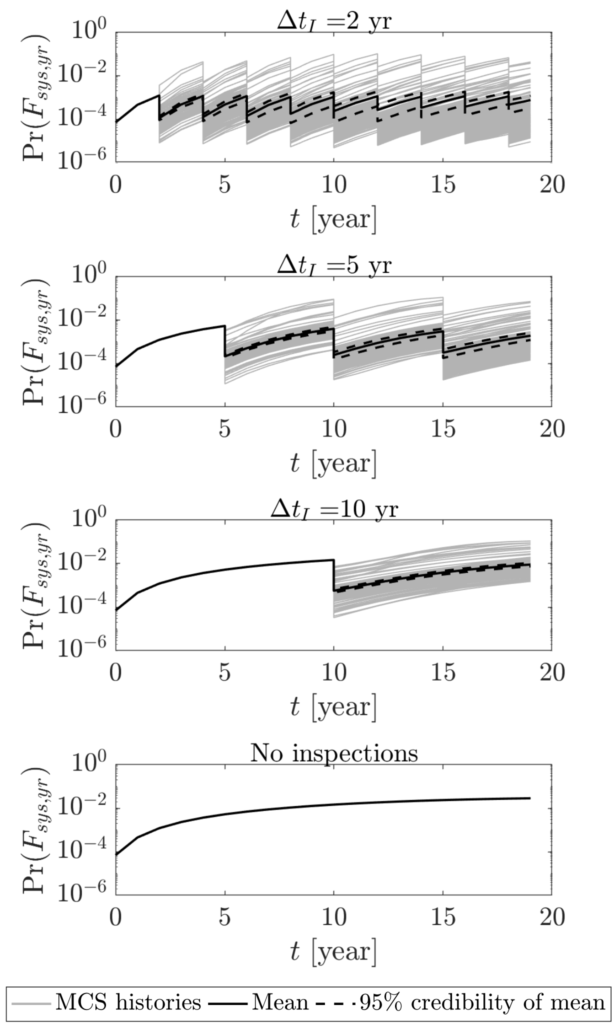

Fig. 13. Time evolution of the annual probability of system failure $\Pr(F_{sys,yr})$ for different inspection intervals Δt_I, with $FDF_d = 2$.

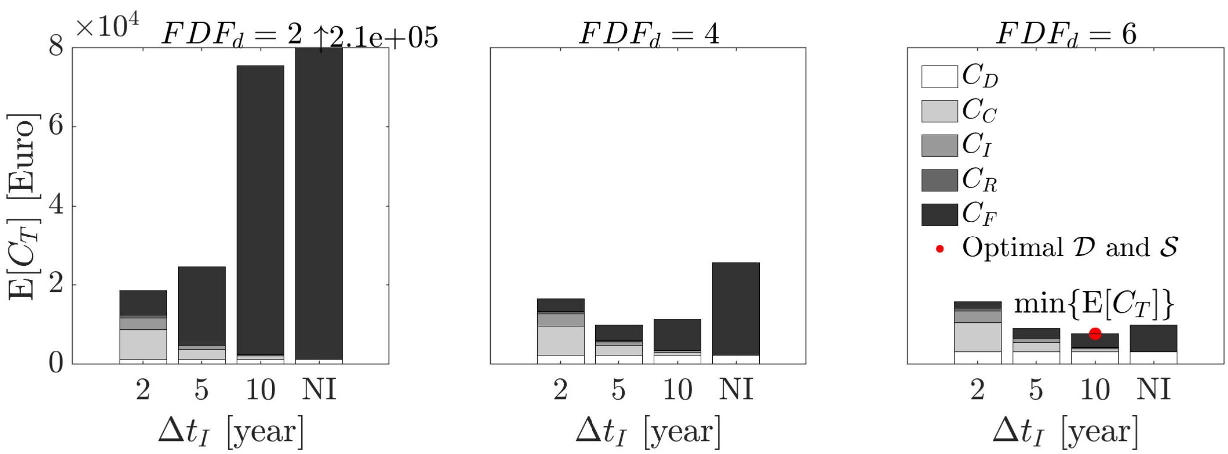

Fig. 14. Expected life-cycle cost E[C_T] for the considered fatigue design factors FDF_d and inspection intervals Δt_I.

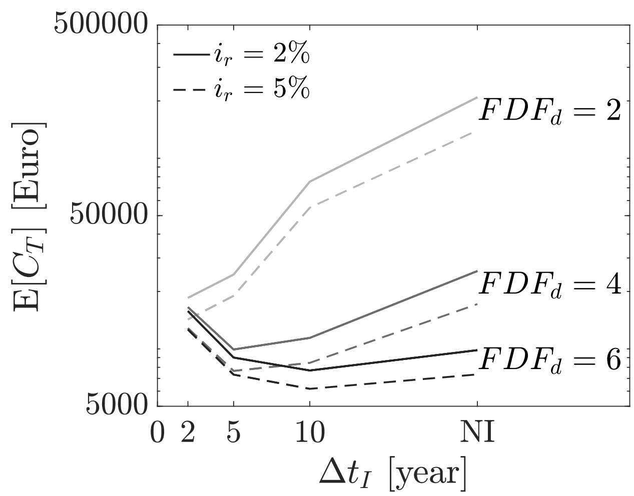

Fig. 15. Influence of the annual discount rate i_r on the expected life-cycle cost E$[C_T]$ and optimal fatigue design factor FDF_d and inspection interval Δt_I.